An efficient multi-dimensional implementation of VSIAM3 and its applications to free surface flows

Kensuke Yokoi[1][*] Mikito Furuichi[2], Mikio Sakai[3]
[1]School of Engineering, Cardiff University, Cardiff, CF24 3AA, UK.
[2]Department of Mathematical Science and Advanced Technology,
Japan Agency for Marine-Earth Science and Technology (JAMSTEC),
3173-25, Showa-machi, Kanazawa, Yokohama, Japan
[3]Resilience Engineering Research Center, School of Engineering,
The University of Tokyo, 7-3-1 Hongo, Bunkyo-ku, Tokyo 113-8656, Japan

October 30, 2017

Abstract

We propose an efficient multidimensional implementation of VSIAM3 (volume/surface integrated average based multi-moment method). Although VSIAM3 is a highly capable fluid solver based on a multi-moment concept and has been used for a wide variety of fluid problems, VSIAM3 could not simulate some simple benchmark problems well (for instance, lid-driven cavity flows) due to relatively high numerical viscosity. In this paper, we resolve the issue by using the efficient multidimensional approach. The proposed VSIAM3 is shown to capture lid-driven cavity flows of Reynolds number up to Re=7500 with a Cartesian grid of 128×128, which was not capable for the original VSIAM3. We also tested the proposed framework in free surface flow problems (droplets collision and separation of We=40, and droplet splashing on a superhydrophobic substrate). The numerical results by the proposed VSIAM3 showed reasonable agreements with these experiments. The proposed VSIAM3 could capture droplets collision and separation of We=40 with a low numerical resolution (8 meshes for the initial diameter of droplets). We also simulated free surface flows including particles toward Non-Newtonian flow applications. These numerical results have showed that the proposed VSIAM3 can robustly simulate interactions among air, particles (solid) and liquid.

[*]Corresponding author: School of Engineering, Cardiff University, The Parade, Cardiff, CF24 3AA, UK, Tel. +44-29-20870844, Fax. +44-29-20874716, YokoiK@cardiff.ac.uk.

1 Introduction

VSIAM3 was invented by Xiao et al. (one-dimensional formulation in 2014 [22] and multi-dimensional formulation in 2015 [25]) [23, 1] and has been used for various fluid problems (incompressible flows, compressible flows, free surface flows, etc.), for instance, milkcrown in 2008 [34], oceanic flow in 2009 [30], droplet impact on dry surface in 2009 [40], droplet splashing on dry surface in 2011 [36, 37, 38], etc. Fig.
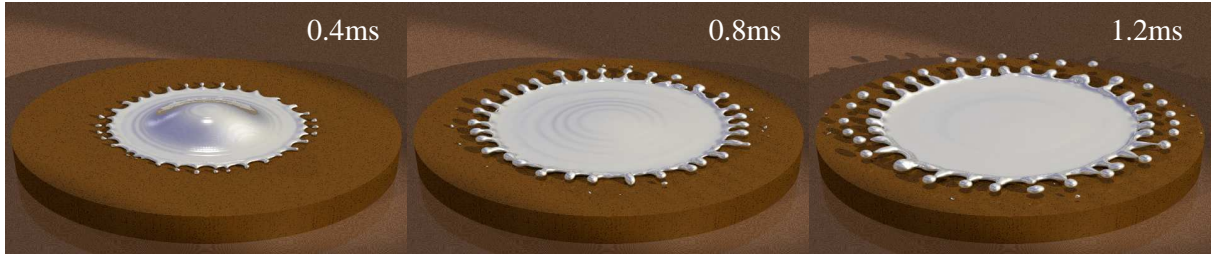

Figure 1: A numerical result by the original VSIAM3. A distilled water droplet of 1.86 [mm] impacts onto a super hydrophobic substrate (the equilibrium angle is $163°$). The droplet impact speed is 2.98 [m/s]. A Cartesian grid of $192 \times 192 \times 48$ and $\alpha = 1.5\Delta x$ are used.

1 shows a typical numerical result of a droplet splashing by VSIAM3. Although a relatively coarse grid (Cartesian grid of $192 \times 192 \times 48$) was used in this simulation, the numerical result has captured the physics of droplet splashing. The numerical simulation was completed within 2 hours using a standard desktop computer (Intel Core i7-3820 3.6GHz, 8GB memory). Although VSIAM3 is a highly capable fluid solver, VSIAM3 could not simulate some simple benchmark problems well (for instance, lid-driven cavity flows of Re>1000 as shown in Section 3) due to relatively high numerical viscosity. The numerical viscosity restricted applications of VSIAM3 to higher Reynolds number flows and/or Non-Newtonian flows. In this paper, we resolve the issue by proposing an efficient multidimensional formulation of VSIAM3.

VSIAM3 is a fluid solver based on a multi-moment concept. Multi-moment method is defined as a method which uses at least two different types of moments (variables) and updates these moments by using different formulations. In standard single-moment methods such as ENO (essentially non-oscillatory) [6] and WENO (weighted ENO) schemes [12, 9], only cell average or boundary (point) value is used as the moment and is updated by a finite difference method or finite volume method. In VSIAM3, both boundary value and cell average are used as moments (i.e. two different moments), and the boundary value and cell average are updated by a finite difference method and finite volume method, respectively (i.e. two different formu-

2

lations). VSIAM3 employs the CIP-CSL (constrained interpolation profile-conservative semi-Lagrangian)

scheme [29, 27, 28, 14, 11] as the conservation equation solver.

In this paper, we improve VSIAM3 by proposing an efficient multi-dimensional implementation of VSIAM3 to resolve the issues on numerical viscosity. In the original VSIAM3, a simple multidimensional framework which is referred to as TEC (Time Evolution Converting) formula [22, 25, 23] based on simple averaging procedures were used. In this paper, we propose a multidimensional formulation which solves the governing equations as much as possible and minimizes the use of such averaging procedures. The details of the multidimensional formulation as well as the original VSIAM3 is given in Section 2. In Section 3, numerical results of lid-driven cavity flows, free surface flows (droplet collision and separation, and droplet splashing) and flows with particles are given. The summary is given in Section 4.

2 Numerical method

In this section, we explain the detail of the original VSIAM3 and propose an efficient multi-dimensional implementation of VSIAM3.

2.1 Outline of VSIAM3 and Grid for VSIAM3 (M-grid)

Here we briefly explain further details of differences between VSIAM3 and typical single-moment methods. Fig. 2 (a) shows a schematic figure of 2D grid. In most of standard single-moment methods, collocation
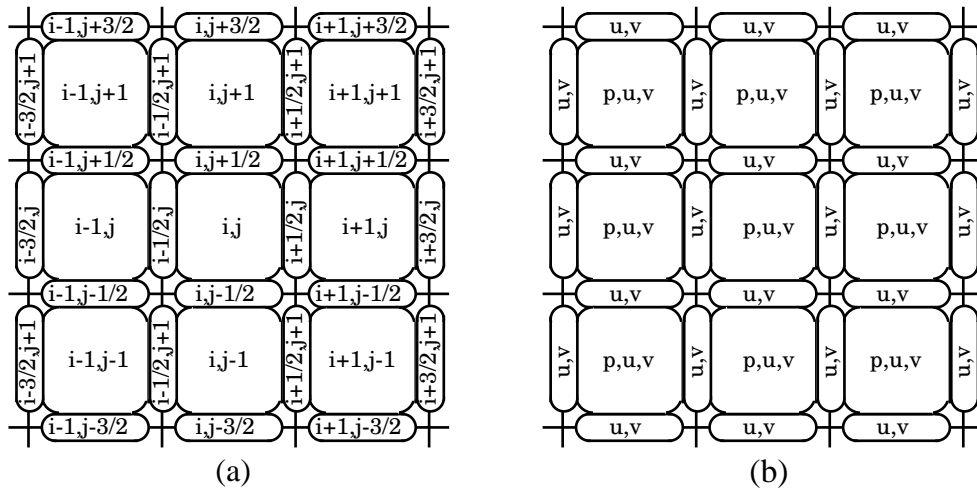

Figure 2: Schematic figure of 2D grid.

or staggered grid is used. When a collocation grid is used, p, u, v are defined at the same location (for instance, at cell center, $p_{i,j}$, $u_{i,j}$, $v_{i,j}$), here p is the pressure, and u and v are x- and y-components of the velocity, respectively. In staggered grid, p, u and v are defined at different locations ($p_{i,j}$ is defined at the cell center, $u_{i+1/2,j}$ on a cell boundary and $v_{i,j+1/2}$ on the other cell boundary). In the multi-moment framework, although p is defined only at the cell center ($p_{i,j}$) like standard single-moment methods, u and v are defined at cell center and on all cell boundaries ($u_{i,j}, u_{i+1/2,j}, u_{i,j+1/2}, v_{i,j}, v_{i+1/2,j}, v_{i,j+1/2}$) as shown in Fig. 2 (b). This grid is called M-grid [26]. These cell average and boundary values are defined as

$$u_{i,j} = \frac{1}{\Delta x \Delta y} \int_{x_{i-1/2}}^{x_{i+1/2}} \int_{y_{j-1/2}}^{y_{j+1/2}} u(x,y)dxdy, \tag{1}$$

$$u_{i-1/2,j} = \frac{1}{\Delta y} \int_{y_{j-1/2}}^{y_{j+1/2}} u(x_{i-1/2},y)dy, \tag{2}$$

$$u_{i,j-1/2} = \frac{1}{\Delta x} \int_{x_{j-1/2}}^{x_{j+1/2}} u(x,y_{j-1/2})dx. \tag{3}$$

In VSIAM3, these additional moments are used in velocity computations and increase the accuracy of velocity calculations. Although the calculation cost of the velocity is increased, when a semi-implicit method which solves the pressure implicitly and velocity explicitly is used (for instance the case of droplet splashing of Fig. 1), the increase of calculation cost by the additional moments is negligible because the pressure calculation is dominating the total calculation time and the number of definition points of pressure is the same with that of single moment method. This multi-moment framework made the efficient calculation of droplet splashing possible. However VSIAM3 requires more memory than other standard methods (3 times for velocity in 2D and 4 times for in 3D).

2.2 Governing equations

In this paper, we consider only incompressible flows and the following governing equations are used

$$\int_\Gamma \mathbf{u} \cdot \mathbf{n}dS = 0, \tag{4}$$

$$\frac{\partial}{\partial t} \int_\Omega \mathbf{u}dV + \int_\Gamma \mathbf{u}(\mathbf{u} \cdot \mathbf{n})dS = -\frac{1}{\rho} \int_\Gamma p\mathbf{n}dS + \frac{1}{\rho} \int_\Gamma \tau \cdot \mathbf{n}dS, \tag{5}$$

where $\mathbf{u}$ is the velocity, $\mathbf{n}$ the outgoing normal for the control volume Ω with its surface denoted by Γ, ρ the density, p the pressure and τ the viscous stress tensor.

4

2.3 Fractional step

A fractional step approach [34] is used as follows:

$$\mathbf{u}^{t+\Delta t} = f^{NA2}(f^{NA1}(f^A(\mathbf{u}^t))), \tag{6}$$

1. advection part (f^A):

$$\frac{\partial}{\partial t}\int_\Omega \mathbf{u}dV + \int_\Gamma \mathbf{u}(\mathbf{u}\cdot\mathbf{n})dS = 0, \tag{7}$$

2. non-advection part 1 (f^{NA1}):

$$\frac{\partial}{\partial t}\int_\Omega \mathbf{u}dV = \frac{1}{\rho}\int_\Gamma \tau\cdot\mathbf{n}dS, \tag{8}$$

3. non-advection part 2 (f^{NA2}):

$$\int_\Gamma \mathbf{u}\cdot\mathbf{n}dS = 0, \tag{9}$$

$$\frac{\partial}{\partial t}\int_\Omega \mathbf{u}dV = -\frac{1}{\rho}\int_\Gamma p\mathbf{n}dS. \tag{10}$$

These equations are solved by VSIAM3, in which the advection part is solved by a CIP-CSL method.

2.4 Advection part (f^A)

A CIP-CSL method is used to solve the conservation equation

$$\frac{\partial}{\partial t}\int_\Omega \phi dV + \int_\Gamma \phi(\mathbf{u}\cdot\mathbf{n})dS = 0, \tag{11}$$

here ϕ is a scalar value. In this paper, the CIP-CSLR method [28] which is a less oscillatory CIP-CSL scheme is used.

2.4.1 CIP-CSLR

The CIP-CSLR scheme is briefly explained here. In the CIP-CSLR method [28], the following function $\Phi_i(x)$

$$\Phi_i(x) = \frac{\alpha_i\beta_i(x-x_{i-1/2})^2 + 2\alpha_i(x-x_{i-1/2}) + \phi_{i-1/2}}{\left(1+\beta_i(x-x_{i-1/2})\right)^2}, \tag{12}$$

is used to interpolate between $x_{i-1/2}$ and $x_{i+1/2}$. The coefficients, α_i and β_i, are determined as follows

$$\alpha_i = \beta_i\phi_i + (\phi_i - \phi_{i-1/2})/\Delta x, \tag{13}$$

$$\beta_i = \frac{1}{\Delta x}\left(\frac{|(\phi_{i-1/2}-\phi_i)|+\varepsilon}{|(\phi_i-\phi_{i+1/2})|+\varepsilon}+1\right), \tag{14}$$

5

by using the following constraints

$$\Phi_i(x_{i+1/2}) = \phi_{i+1/2}, \tag{15}$$

$$\phi_i = \int_{x_{i-1/2}}^{x_{i+1/2}} \Phi_i(x)dx/\Delta x. \tag{16}$$

Here ε is a small number to avoid zero division. We used $\varepsilon = 10^{-15}$ for all results in this paper. By using the interpolation function $\Phi_i(x)$, the boundary value $\phi_{i-1/2}$ can be updated by the conservation equation of a differential form

$$\frac{\partial \phi}{\partial t} + u\frac{\partial \phi}{\partial x} = -\phi\frac{\partial u}{\partial x}. \tag{17}$$

Eq. (17) is solved using a splitting approach as follows

$$\frac{\partial \phi}{\partial t} + u\frac{\partial \phi}{\partial x} = 0, \tag{18}$$

$$\frac{\partial \phi}{\partial t} = -\phi\frac{\partial u}{\partial x}. \tag{19}$$

A semi-Lagrangian approach is used for the advection equation (18)

$$\phi_{i-1/2}^* = \begin{cases} \Phi_{i-1}(x_{i-1/2} - u_{i-1/2}\Delta t) & \text{if} \quad u_{i-1/2} \geq 0 \\ \Phi_i(x_{i-1/2} - u_{i-1/2}\Delta t) & \text{if} \quad u_{i-1/2} < 0. \end{cases} \tag{20}$$

Eq. (19) is solved by a finite difference method [1]. The cell average ϕ_i is updated by a finite volume formulation

$$\phi_i^{n+1} = \phi_i^n - \frac{F_{i+1/2} - F_{i-1/2}}{\Delta x}, \tag{21}$$

here $F_{i-1/2}$ is the flux

$$F_{i-1/2} = \begin{cases} -\int_{x_{i-1/2}}^{x_{i-1/2} - u_{i-1/2}\Delta t} \Phi_{i-1}(x)dx & \text{if} \quad u_{i-1/2} \geq 0 \\ -\int_{x_{i-1/2}}^{x_{i-1/2} - u_{i-1/2}\Delta t} \Phi_i(x)dx & \text{if} \quad u_{i-1/2} < 0. \end{cases} \tag{22}$$

The detail description can be found in [28].

2.4.2 Original multi-dimensional formulation (TEC formula)

In the original VSIAM3, a dimensional splitting method [25, 22] is used for CIP-CSL scheme. Fig. 3 shows the schematic figure of the multi-dimensional formulation in 2D. For x-direction, $\phi_{i,j}^*$ and $\phi_{i-1/2,j}^*$ are firstly updated from $\phi_{i,j}^n$ and $\phi_{i-1/2,j}^n$ by using the 1D CIP-CSL solver (Step 1 in Fig. 3). However some boundary values such as $\phi_{i,j-1/2}^n$ cannot be updated using the 1D CIP-CSL solver because there are no boundary values
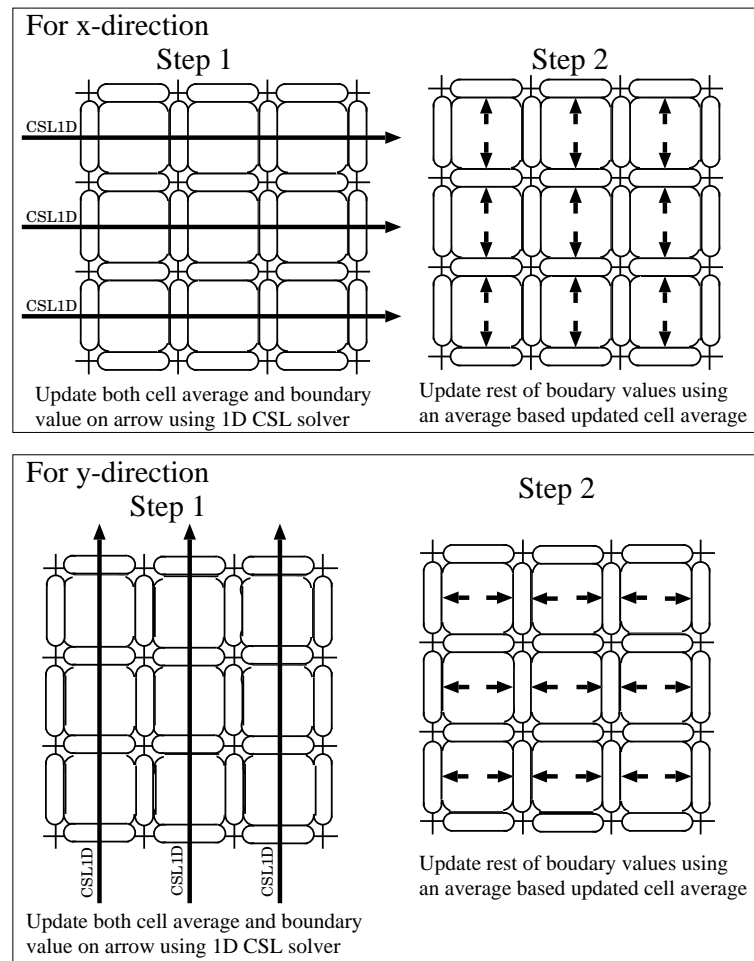
6

For x-direction

Step 1

CSL1D

CSL1D

CSL1D

Update both cell average and boundary value on arrow using 1D CSL solver

Step 2

Update rest of boudary values using an average based updated cell average

For y-direction

Step 1

CSL1D   CSL1D   CSL1D

Update both cell average and boundary value on arrow using 1D CSL solver

Step 2

Update rest of boudary values using an average based updated cell average

Figure 3: Schematic figures of the dimensional splitting approach using the TEC formula.

$(\phi_{i-1/2,j-1/2}$ and $\phi_{i+1/2,j-1/2})$ for $\phi_{i,j-1/2}$. Therefore $\phi_{i,j-1/2}^n$ is updated by the TEC formula (Step 2) without solving the conservation equation, as follows:

$$\phi_{i,j-1/2}^* = \phi_{i,j-1/2}^n + \frac{1}{2}(\phi_{i,j}^* - \phi_{i,j}^n + \phi_{i,j-1}^* - \phi_{i,j-1}^n). \tag{23}$$

A similar approach is used for y-direction. $\phi_{i,j}^{n+1}$ and $\phi_{i,j-1/2}^{n+1}$ are computed from $\phi_{i,j}^*$ and $\phi_{i-1/2,j}^*$ by using a 1D CIP-CSL method. $\phi_{i-1/2,j}^*$ is updated by TEC as follows:

$$\phi_{i-1/2,j}^{n+1} = \phi_{i-1/2,j}^* + \frac{1}{2}(\phi_{i,j}^{n+1} - \phi_{i,j}^* + \phi_{i-1,j}^{n+1} - \phi_{i-1,j}^*). \tag{24}$$

Although the TEC formula seems to be a monotone operation, TEC causes numerical oscillations even the 1D CSL scheme is oscillation free as shown in Section 3.

2.4.3   Proposed multi-dimensional formulation (TM formula)

Here we propose a different type of dimensional splitting formulation which solves the equation for all moments by creating temporary moments (TMs). When the 1D solver is used for x-direction, we could not update $\phi_{i,j-1/2}$ because there are no boundary values for $\phi_{i,j-1/2}$. Therefore we calculate TMs using a simple interpolation:

$$\phi_{i-1/2,j-1/2}^n = \frac{1}{2}(\phi_{i,j-1/2}^n + \phi_{i-1,j-1/2}^n), \tag{25}$$

as shown in Fig. 4 (Step 1). Once TMs are calculated, the 1D CIP-CSL solver can be used to update $\phi_{i,j-1/2}$ (Step 2). After $\phi_{i,j-1/2}$ is updated, TMs are abandoned. Hereinafter the multi-dimensional approach referred to as TM formula. For y-direction, the procedure is almost same with that for x-direction. $\phi_{i,j}$, $\phi_{i,j-1/2}$ and $\phi_{i,j+1/2}$ are updated by the 1D CIP-CSL solver. For $\phi_{i-1/2,j-1/2}$, we firstly calculate TMs using

$$\phi_{i-1/2,j-1/2}^* = \frac{1}{2}(\phi_{i-1/2,j}^* + \phi_{i-1/2,j-1}^*), \tag{26}$$

then use the 1D CIP-CSL solver. The implementation of this multi-dimensional approach is simple and the extension to 3D is also straightforward. TM does not cause numerical oscialltions if the 1D scheme is oscialltion free.

Summary of the procedure:

x-direction

  1. Calculate TMs as $\phi_{i-1/2,j-1/2} = (\phi_{i,j-1/2} + \phi_{i-1,j-1/2})/2$ and $u_{i-1/2,j-1/2} = (u_{i,j-1/2} + u_{i-1,j-1/2})/2$.
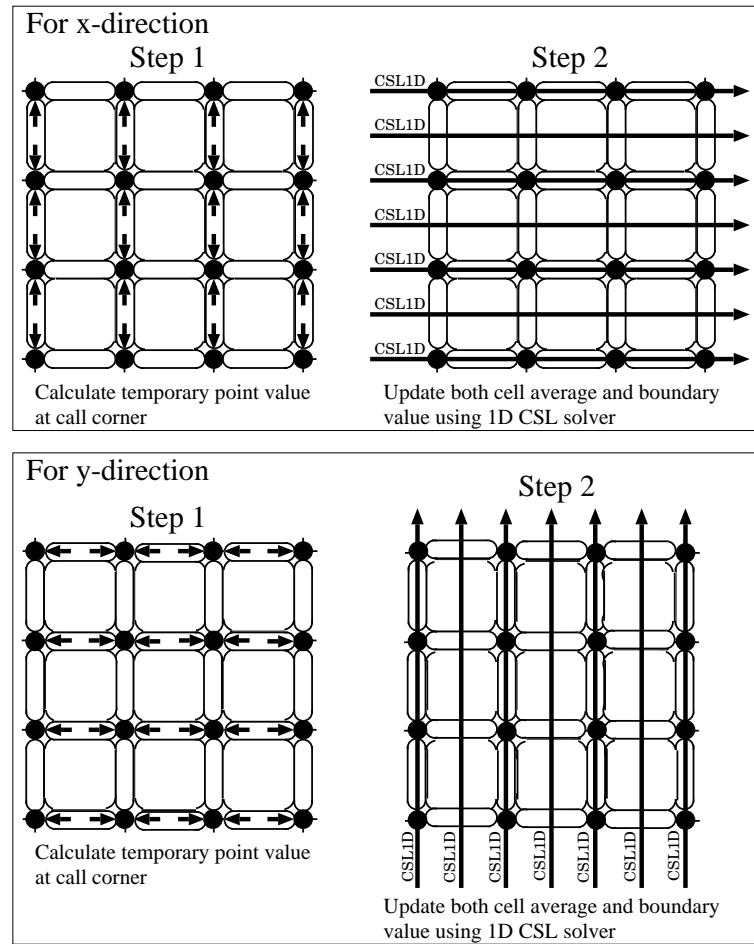
8

For x-direction

Step 1

Calculate temporary point value at call corner

Step 2

CSL1D
CSL1D
CSL1D
CSL1D
CSL1D
CSL1D
CSL1D

Update both cell average and boundary value using 1D CSL solver

For y-direction

Step 1

Calculate temporary point value at call corner

Step 2

CSL1D CSL1D CSL1D CSL1D CSL1D CSL1D CSL1D

Update both cell average and boundary value using 1D CSL solver

Figure 4: Schematic figures of the dimensional splitting approach using the TM formula.

132 2. Update all moments ($\phi_{i,j}$, $\phi_{i-1/2,j}$, $\phi_{i+1/2,j}$, $\phi_{i,j-1/2}$ and $\phi_{i,j+1/2}$) using 1D CIP-CSL solver.

133 **y-direction**

134 1. Calculate TMs as $\phi_{i-1/2,j-1/2} = (\phi_{i-1/2,j} + \phi_{i-1/2,j-1})/2$ and $u_{i-1/2,j-1/2} = (u_{i-1/2,j} + u_{i-1/2,j-1})/2$.

135 2. Update all moments ($\phi_{i,j}$, $\phi_{i,j-1/2}$, $\phi_{i,j+1/2}$, $\phi_{i-1/2,j}$ and $\phi_{i+1/2,j}$) using 1D CIP-CSL solver.

2.5 Non-advection Part 1 (f^{NA1})

137 The viscosity term is computed by a standard finite volume formulation for cell averages.

$$\frac{1}{\rho} \int_{\Gamma} \tau \cdot \mathbf{n} dS = \frac{1}{\rho_{i,j}} \left(\frac{\tau_{i+1/2,j} - \tau_{i-1/2,j}}{\Delta x} + \frac{\tau_{i,j+1/2} - \tau_{i,j-1/2}}{\Delta y} \right). \tag{27}$$

138 Although, in the original VSIAM3, the boundary values were updated by TEC, in this paper, we solve Eq.
139 (27) for the boundary values. We simply used a standard discretization for the boundary values as well.
140 For instance, the following second-order central difference scheme is used for all moments in cases of two
141 dimensional single phase flows,

$$u_{i,j} = u_{i,j} + \frac{\mu}{\rho} \left(\frac{u_{i+1,j} + u_{i-1,j} - 2u_{i,j}}{\Delta x^2} + \frac{u_{i,j+1} + u_{i,j-1} - 2u_{i,j}}{\Delta y^2} \right) \Delta t, \tag{28}$$

142

$$u_{i-1/2,j} = u_{i-1/2,j} + \frac{\mu}{\rho} \left(\frac{u_{i+1/2,j} + u_{i-3/2,j} - 2u_{i-1/2,j}}{\Delta x^2} + \frac{u_{i-1/2,j+1} + u_{i-1/2,j-1} - 2u_{i-1/2,j}}{\Delta y^2} \right) \Delta t, \tag{29}$$

143

$$u_{i,j-1/2} = u_{i,j-1/2} + \frac{\mu}{\rho} \left(\frac{u_{i+1,j-1/2} + u_{i-1,j-1/2} - 2u_{i,j-1/2}}{\Delta x^2} + \frac{u_{i,j-3/2} + u_{ij+1/2} - 2u_{i,j-1/2}}{\Delta y^2} \right) \Delta t. \tag{30}$$

144

2.6 Non-advection Part 2 (f^{NA2})

146 By combining the divergence of Eq. (10) and $\int_{\Gamma} \mathbf{u}^{n+1} \cdot \mathbf{n} dS = 0$, the following Poisson equation

$$\int_{\Gamma} \frac{\nabla p^{n+1}}{\rho} \cdot \mathbf{n} dS = \frac{1}{\Delta t} \int_{\Gamma} \mathbf{u}^* \cdot \mathbf{n} dS, \tag{31}$$

147 is obtained, where $\mathbf{u}^*$ is the velocity after non-advection part 1. Eq. (31) was discretized as

$$\begin{aligned}
&\frac{(\frac{1}{\rho_{i+1/2,j}^{n+1}} \partial_x p^{n+1})_{i+1/2,j} - (\frac{1}{\rho_{i-1/2,j}^{n+1}} \partial_x p^{n+1})_{i-1/2,j}}{\Delta x} \\
&+ \frac{(\frac{1}{\rho_{i,j+1/2}^{n+1}} \partial_y p^{n+1})_{i,j+1/2} - (\frac{1}{\rho_{i,j-1/2}^{n+1}} \partial_x p^{n+1})_{i,j-1/2}}{\Delta y} \\
&= \frac{1}{\Delta t} \left(\frac{u_{i+1/2,j}^* - u_{i-1/2,j}^*}{\Delta x} + \frac{v_{i,j+1/2}^* - v_{i,j-1/2}^*}{\Delta y} \right),
\end{aligned} \tag{32}$$

10

here

$$\left(\frac{1}{\rho_{i-1/2,j}^{n+1}}\partial_x p^{n+1}\right)_{i-1/2,j} \equiv \frac{2}{\rho_{i,j}^{n+1}+\rho_{i-1,j}^{n+1}}\frac{p_{i,j}^{n+1}-p_{i-1,j}^{n+1}}{\Delta x}. \tag{33}$$

A preconditioned conjugate gradient (CG) method is used for the pressure Poisson equation. The convergence tolerance of the pressure Poisson equation $\varepsilon_p = 10^{-10}$ is used. By using p^{n+1}, the boundary values of the velocity are updated as follows

$$u_{i-1/2,j}^{n+1} = u_{i-1/2,j}^* - \frac{\Delta t}{\rho_{i-1/2,j}}\left(\partial_x p^{n+1}\right)_{i-1/2,j}, \tag{34}$$

$$v_{i,j-1/2}^{n+1} = v_{i,j-1/2}^* - \frac{\Delta t}{\rho_{i,j-1/2}}\left(\partial_y p^{n+1}\right)_{i,j-1/2}. \tag{35}$$

Other velocity components ($u_{i,j}$, $v_{i,j}$, $u_{i,j-1/2}$, $v_{i-1/2,j}$) are updated by the TEC formula. Concerning the pressure gradient term, we use the TEC formula in the proposed formulation.

3 Numerical results

We validated the proposed framework through two-dimensional sine wave propagation, Zalesak problem, invicid horizontal shear layer problem, lid-driven cavity flow problems (Re=1000, 3200, 5000 and 7500) and comparisons with experiments (droplet collision and separation [2], and droplet splashing [21]). We also conducted numerical simulations of free surface flows with particles (interactions among air, liquid and particles) as possible Non-Newtonian applications of the proposed framework.

3.1 Two-dimensional sine wave propagation

In this test, two-dimensional conservation equation is solved using the TEC formula and TM formula. The initial condition is

$$\phi(x,y,0) = \sin(2\pi(x+y)), \tag{36}$$

$$\mathbf{u}(x,y) = (1,1). \tag{37}$$

The domain $[0,1] \times [0,1]$ and periodic boundary condition are used. Three different grid sizes $[(N \times N) = (50 \times 50), (100 \times 100)$ and $(200 \times 200)]$ are used with $\Delta x = \Delta y = 1/N$ and $\Delta t = 0.2\Delta x$. Error is defined as follow

$$L_1 = \frac{1}{N}\sum_{i=1}^{N}|\phi_i - \phi_{exact,i}|. \tag{38}$$

11

Table 1: Errors in two-dimensional sine wave propagation at $t = 1$ when the CIP-CSLR method was used.

	Original formulation (TEC)		Proposed formulation (TM)	
	L_1 error	Order	L_1 error	Order
50×50	2.10×10^{-3}	-	2.26×10^{-3}	-
100×100	1.12×10^{-3}	0.91	9.04×10^{-4}	1.32
200×200	6.83×10^{-4}	0.71	3.79×10^{-4}	1.25

Table 1 shows the numerical results. Basically TM is superior to TEC. Although both orders of accuracy are less than second-order, this is due to the 1D CIP-CSLR scheme which includes a type of a limiter (the order of accuracy of CSLR in 1D sine wave test is about 1.5). Therefore we also conducted another convergence study using the CIP-CSL2 scheme [29] which has third-order accuracy in 1D sine wave test (but we do not use the CIP-CSL2 scheme for fluid simulations because the scheme is not oscillation free). Table 2 shows results by the CIP-CSL2 scheme with TEC and TM. Then both results show more than second-order

Table 2: Errors in two-dimensional sine wave propagation at $t = 1$ when the CIP-CSL2 method was used.

	Original formulation (TEC)		Proposed formulation (TM)	
	L_1 error	Order	L_1 error	Order
50×50	5.18×10^{-5}	-	2.65×10^{-5}	-
100×100	1.12×10^{-5}	2.21	4.96×10^{-6}	2.42
200×200	2.63×10^{-6}	2.09	9.85×10^{-7}	2.33

accuracy. Although TM as well as TEC reduces the order of accuracy of 1D CSL-CSL2 scheme because of the interpolation and time splitting, both maintains more than second-order if the 1D solver has 3rd order accuracy.

3.2 Zalesak problem

Zalesak's test problem [41] in which a notched circle is rotated is widely used as a test of scalar advection method. The initial condition is given by

$$\phi = \begin{cases} 1 & \text{if} \quad \sqrt{(x-0.5)^2 + (y-0.75)^2} < 0.17 \text{ and } (y > 0.85 \text{ or } |x-0.5| > 0.03) \\ 0 & \text{if} \quad \text{others,} \end{cases} \tag{39}$$

$$\mathbf{u}(x,y) = (y - 0.5, 0.5 - x). \tag{40}$$

The one revolution is completed with 628 time steps. Fig. 5 shows numerical results (top view of 0.5-contour) by the CIP-CSLR scheme with TEC and TM after one revolution. Both results show good agree-
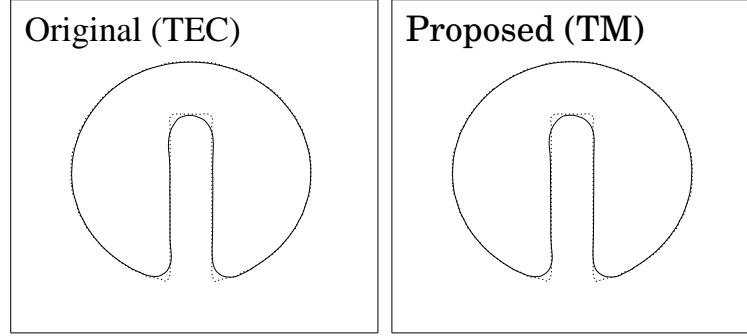

Figure 5: Top views of numerical results of Zalesak problem after one revolution by VSIAM3 using TEC and TM. The solid and dot lines represent 0.5 contour lines of numerical results and exact solution, respectively. The grid of 100×100 was used.

ment with the exact solution. Fig. 6 shows the side views. Although both results are apparently similar, these

results have shown that TEC is not oscillation free and more diffusive than TM, as shown in Fig. 6 (b), (c),

(e) and (f). TM is oscillation free.

3.3   Invicid horizontal shear layer problem

In this subsection, Euler equation is solved using VSIAM3 with TM and TEC. The flow consists of a hor-

izontal shear layer of finite thickness with small vertical perturbation [3]. The initial condition is given

by

$$u(x,y) = \begin{cases} \tanh(30(y - \frac{1}{4})) & \text{if} \quad y \leq \frac{1}{2} \\ \tanh(30(\frac{3}{4} - y)) & \text{if} \quad y > \frac{1}{2}, \end{cases} \tag{41}$$

$$v(x,y) = \frac{1}{20}\sin(2\pi x). \tag{42}$$

Figures 7 and 8 show numerical results (vorticity contours) by the original VSIAM3 (TEC) and proposed

VSIAM3 (TM), respectively. A Cartesian grid of 128×128 was used in this test.   Both results show

reasonable agreements with the reference (Fig. 1 in [3]). However the result by the original VSIAM3 seems

to be disturbed by numerical oscillations, for instance, see the location indicated by the arrow in Fig. 7

(t=1.8). On the other hand, the result by the proposed VSIAM3 is smoother and closer to the reference(Fig.
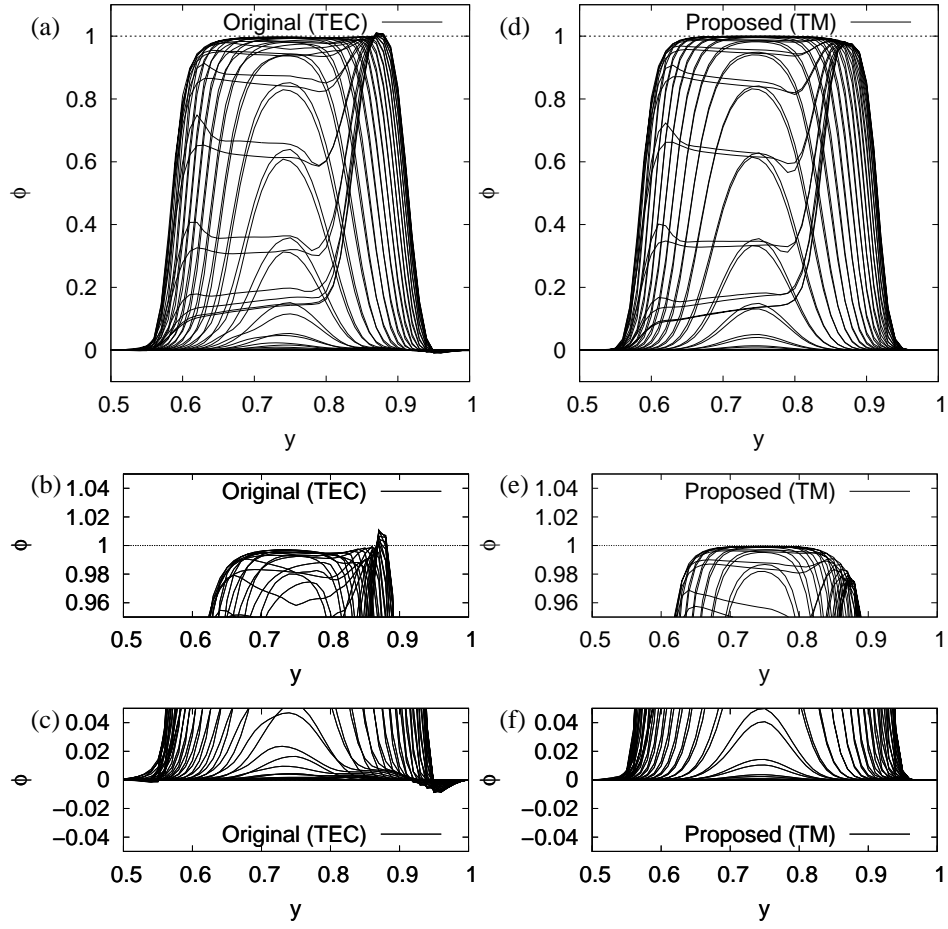
1 [3]).

13

Figure 6: Side views of numerical results of Zalesak problem after one revolution by original VSIAM3 using TEC (a-c) and proposed VSIAM3 using TM (d-f). The grid of 100×100 was used.
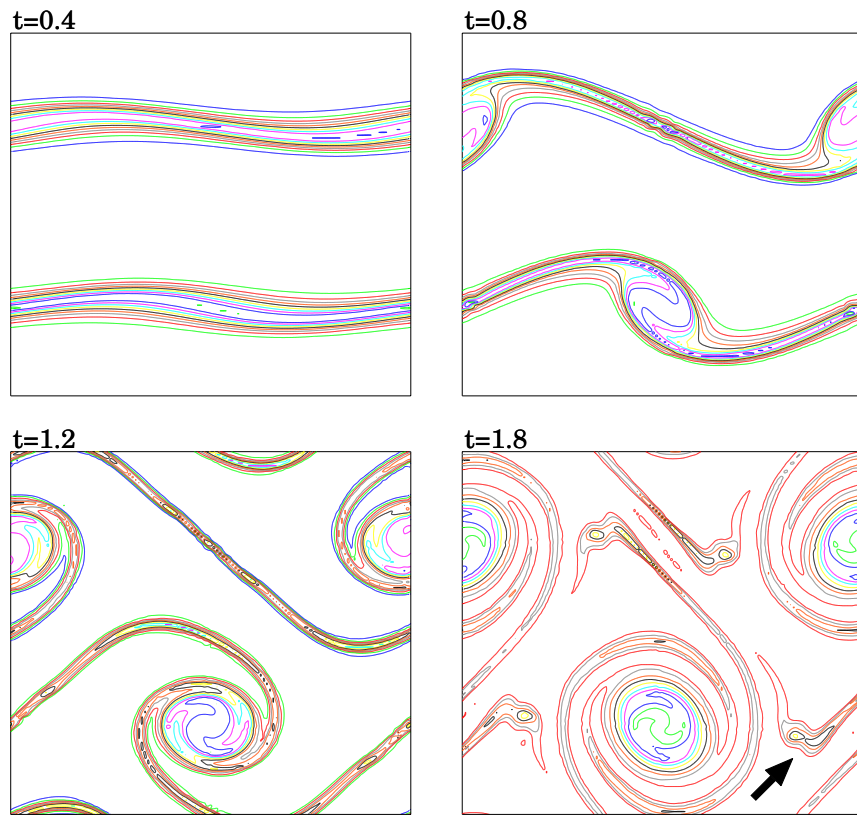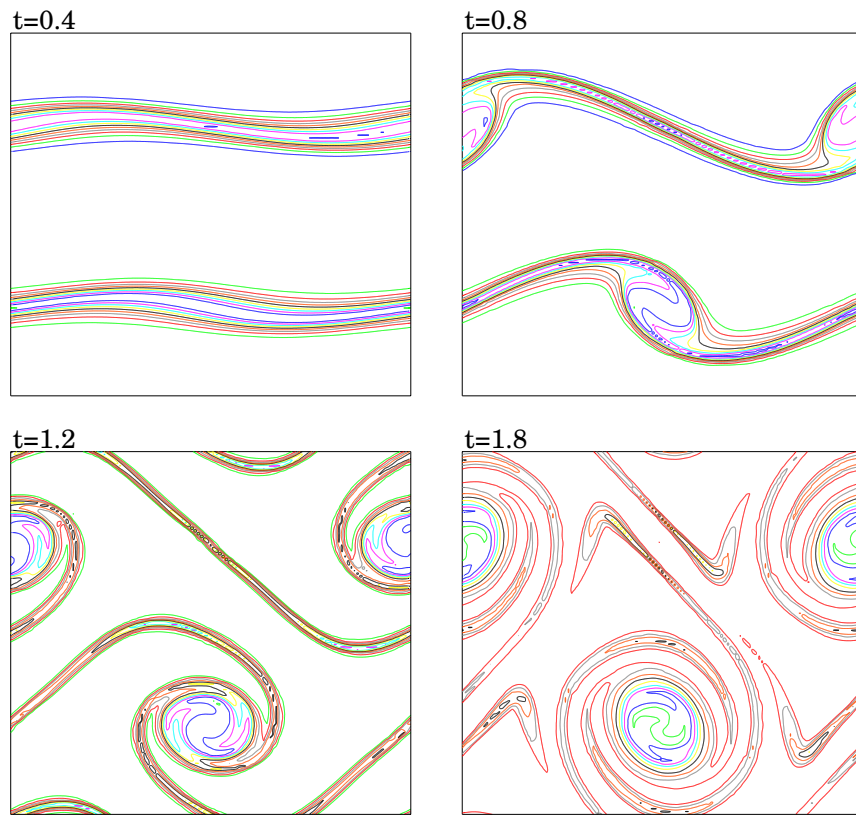
Figure 7: Numerical result of invicid horizontal shear layer problem by the original VSIAM3 (TEC). A Cartesian grid of 128×128 was used. Lines represent vorticity contours of ± 3, ± 6, ± 9, ± 12, ± 15, ± 18, ± 21, ± 24, ± 27 and ± 30.

Figure 8: Numerical result of invicid horizontal shear layer problem by the proposed VSIAM3 (TM). A Cartesian grid of 128×128 was used. Lines represent vorticity contours.

Fig. 9 show time histories of the kinetic energy which is defined as follow

$$K = \int \mathbf{u} \cdot \mathbf{u} dx dy. \tag{43}$$

Error in kinetic energy is slightly improved by the proposed VSIAM3. However loss of kinetic energy is

Figure 9: Kinetic energy versus time for shear layer on 128×128 grid. Kinetic energy has been normalized based on the initial kinetic energy.

still larger than that by the second-order project method [3].

3.4 2D incompressible flows (lid-driven cavity flows)

The proposed and original VSIAM3 were applied to lid-driven cavity flow problems and these numerical results are compared with numerical results by Ghia et al. [5]. Figures 10 and 11 show numerical results of Re= 1000, 3200, 5000 and 7500 by the original VSIAM3 and the proposed VSIAM3, respectively. Although the original VSIAM3 could simulate the cavity flow of Re=1000 with the grid of 128×128 as shown in Fig. 10, could not accurately simulate cavity flows of Re=3200, 5000 and 7500 due to high numerical viscosity. Fig. 11 shows the numerical results by the proposed VSIAM3. These results have shown that the proposed VSIAM3 can capture cavity flows up to Re=7500 by improving numerical viscosity.

Figures 12 and 13 show numerical results of convergence studies of lid-driven cavity flows of Re= 5000 and 7500 by the original VSIAM3 and proposed VSIAM3, respectively. When 256×256 grid is used, the original VSIAM3 could also capture the cavity flow of Re=5000 well, however could not accurately capture

17
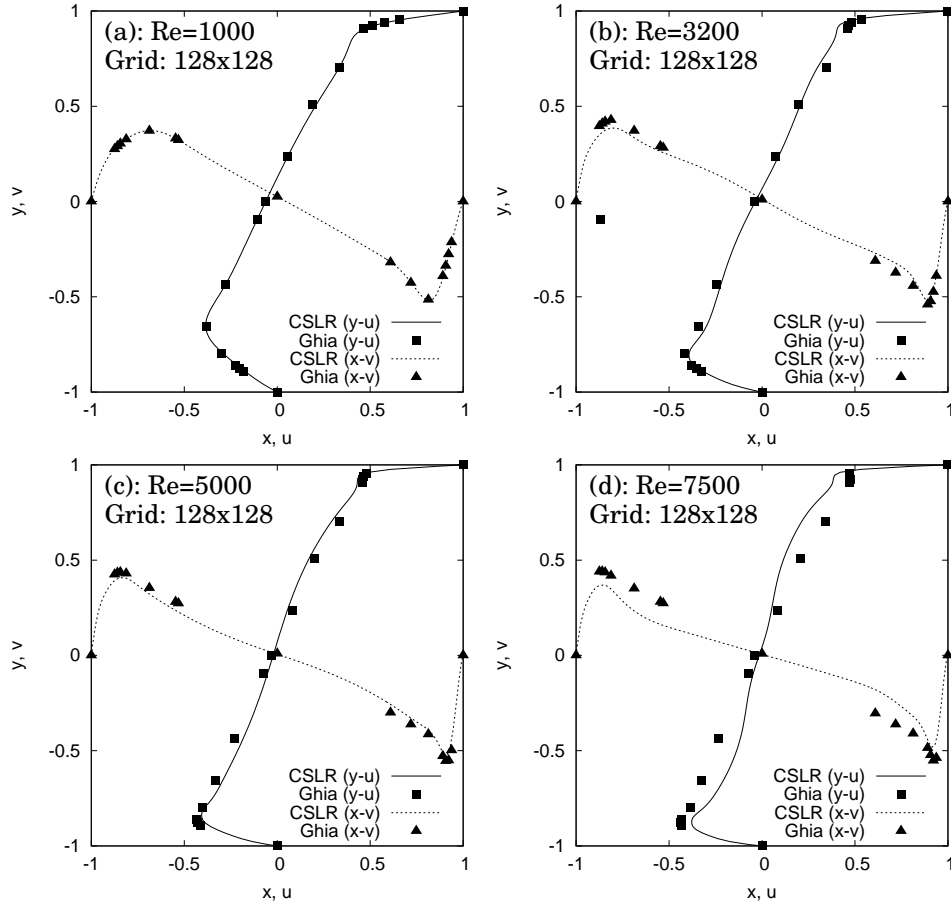
Figure 10: Numerical results of lid-driven cavity flows of Re=1000, 3200, 5000 and 7500 by the original VSIAM3. A Cartesian grid of 128×128 was used. The solid and dot lines represent x- and y- components of the velocity fields on the lines $x = 0$ and $y = 0$, respectively. Dots represent numerical results by Ghia et al. [5].
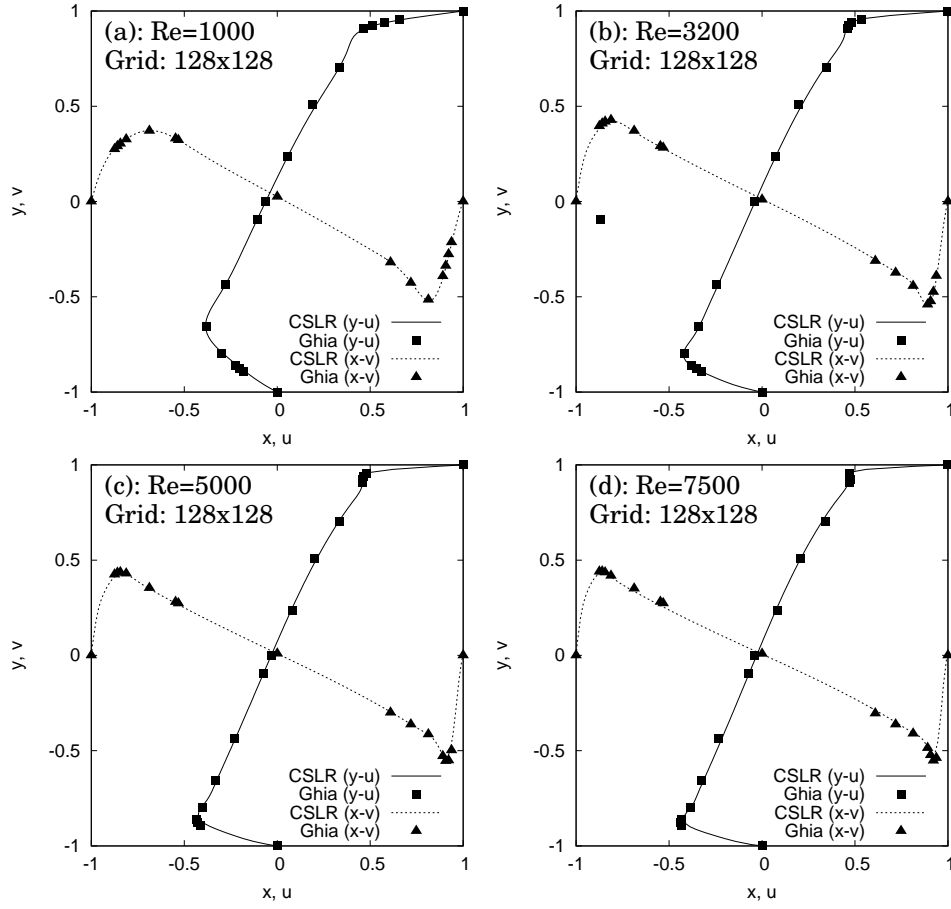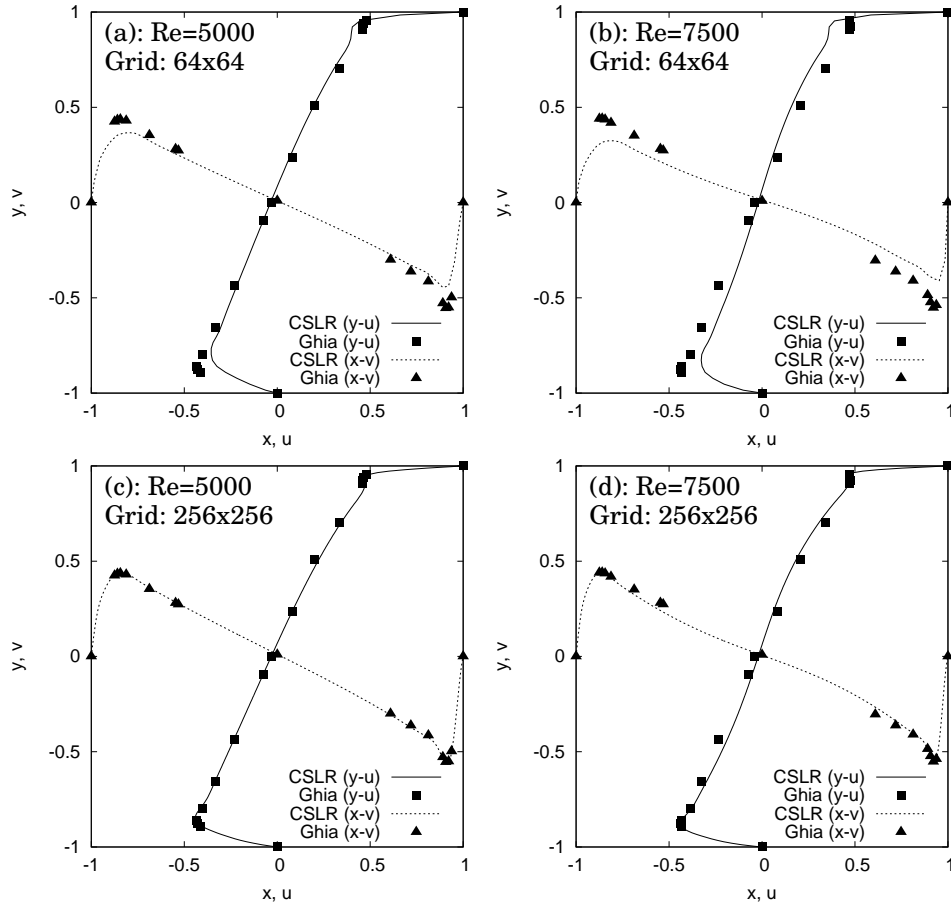
Figure 11: Numerical results of lid-driven cavity flows of Re=1000, 3200, 5000 and 7500 by the proposed VSIAM3. A Cartesian grid of 128×128 was used. The solid and dot lines represent x- and y- components of the velocity fields on the lines $x = 0$ and $y = 0$, respectively. Dots represent numerical results by Ghia et al. [5].

Figure 12: Numerical results of a convergence study of lid-driven cavity flows of Re= 5000 and 7500 by the original VSIAM3. Cartesian grids of 64×64 and 256×256 were used. The solid and dot lines represent x- and y- components of the velocity fields on the lines $x = 0$ and $y = 0$, respectively. Dots represent numerical results by Ghia et al. [5].
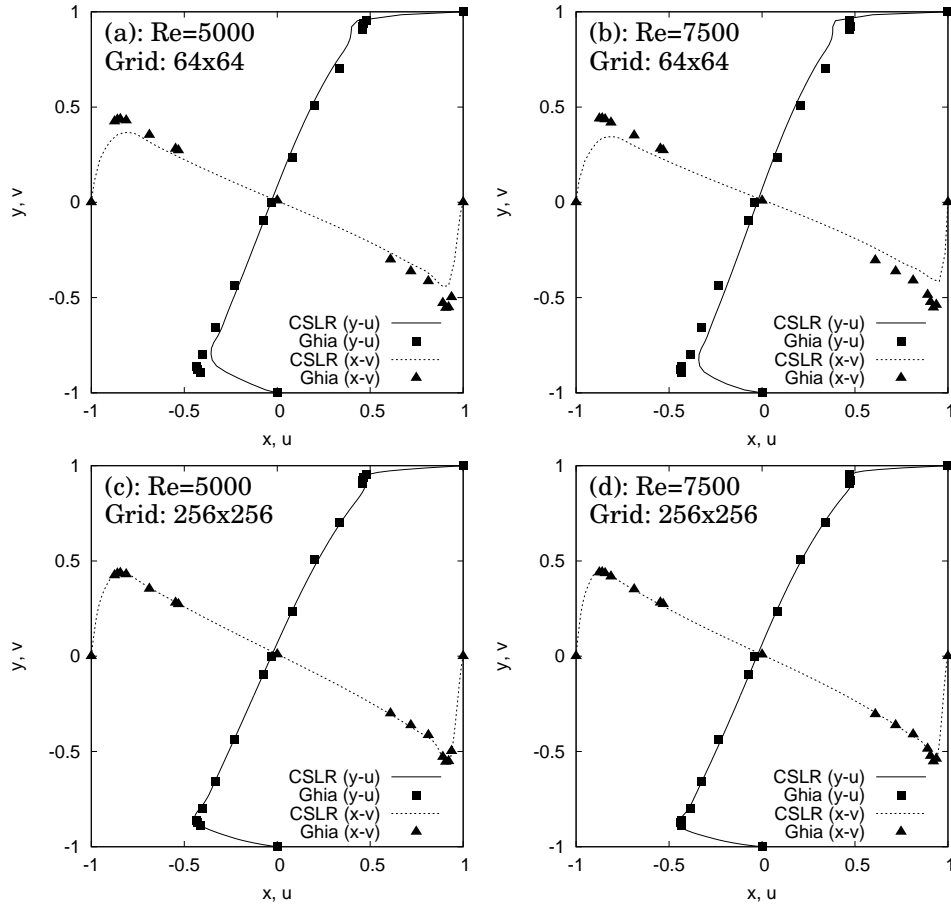
Figure 13: Numerical results of a convergence study of lid-driven cavity flows of Re= 5000 and 7500 by the proposed VSIAM3. Cartesian grids of 64×64 and 256×256 were used. The solid and dot lines represent x- and y- components of the velocity fields on the lines $x = 0$ and $y = 0$, respectively. Dots represent numerical results by Ghia et al. [5].

the cavity flow of Re=7500 as shown in Fig. 12 (c-d). Overall the original VSIAM3 has shown a reasonable convergence for cavity flows of Re=5000 and 7500 as shown in figures 10 and 12. The proposed VSIAM3 could simulate both cavity flows of Re=5000 and 7500 well on 256×256 grid and has shown a reasonable convergence as shown in figures 11 and 13.

3.5 Two droplets collision and separation

We conducted 3D numerical simulations of a free surface flow which includes topology change of liquid interfaces (two droplets collision and separation) [2]. The numerical formulation to simulate free surface flows is based on VSIAM3, the CLSVOF (coupled level set [15, 19] and volume-of-fluid [7, 10]) method [18, 31], the THINC/WLIC (tangent of hyperbola for interface capturing/weighted line interface calculation) scheme [24, 33, 8] and the density scaled balanced continuum surface force model [38, 39] with level set curvature correction [37]. For the full details of the implementation the free surface flow solver, see [34, 37, 38])

Fig. 14 shows snapshots of the numerical results of We=40 by the original VSIAM3 and the proposed VSIAM3 with these of the experiment [2]. In these numerical simulations, quantitative parameters were used. The density ratio is 1.25:1000 (air:liquid). The mesh size $\Delta = D/14$ was used, here D is the diameter of initial droplets. In this numerical resolution, both original and proposed VSIAM3 could capture the phenomenon well.

Fig. 15 show numerical results when a lower numerical resolution, $\Delta = D/8$, was used. Although the proposed VSIAM3 could capture the droplet separation with this lower numerical resolution, the original VSIAM3 failed. The difference could be attributed to the higher numerical viscosity of the original VSIAM3. The original VSIAM3 could capture the phenomenon with $\Delta = D/10$ but failed with $\Delta = D/9$. Although the cost improvement with 2 meshes (about 20%) in one direction sounds small, we can possibly reduce total mesh number about 50% ($0.8 \times 0.8 \times 0.8 = 0.512$) in 3D simulations and also take a larger Δt. Although there are several previous work of this type of numerical simulations [20, 13], to our best knowledge, no other numerical framework can capture the phenomenon with this low numerical resolution.
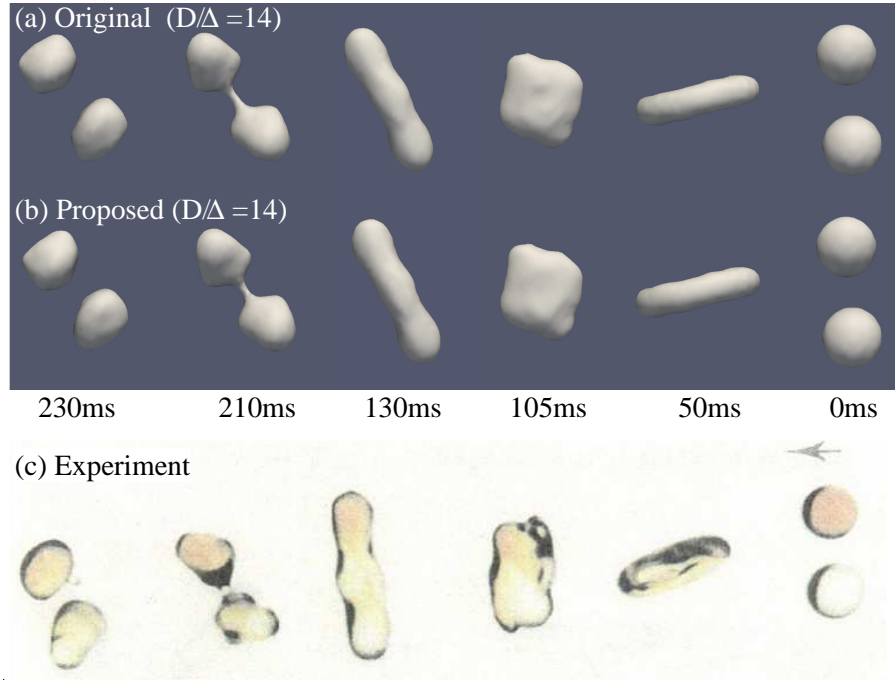
Figure 14: Numerical results of two droplet collision and separation by the original VSIAM3 (a) and proposed VSIAM3 (b) with the experiment of We=40 (c) [2]. The time evolution is from right to left. The mesh size is $\Delta = D/14$. Reproduced with permission from Journal of Fluid Mechanics 221, 183-204 (1990). Copyright 1990 Cambridge University Press.
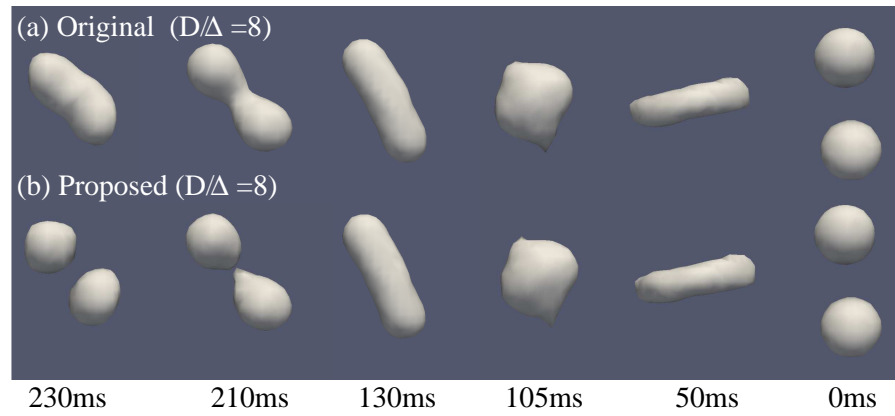

Figure 15: Numerical results of two droplet collision and separation by the original VSIAM3 (a) and proposed VSIAM3 (b). The time evolution is from right to left. The mesh size is $\Delta = D/8$.

3.6 Droplet splashing on superhydrophobic substrate

We performed numerical simulations of prompt splashing using the original and proposed methods, and compared these numerical results with the experiment [21]. In the comparison, quantitative parameters, the densities $\rho_{liquid} = 1000$ kg/m^3, $\rho_{air} = 1.25$ kg/m^3, viscosities $\mu_{liquid} = 1.0 \times 10^{-3}$ Pa·s, $\mu_{air} = 1.82 \times 10^{-5}$ Pa·s, surface tension $\sigma = 7.2 \times 10^{-2}$ N/m, gravity 9.8 m/s^2, initial droplet diameter $D = 1.86$ mm, impact speed 2.98 m/s and the equilibrium contact angle 163° are used. A Cartesian grid of $192 \times 192 \times 48$ is used. Fig. 16 shows the result. The proposed VSIAM3 captures the physics of droplet splashing including satellite
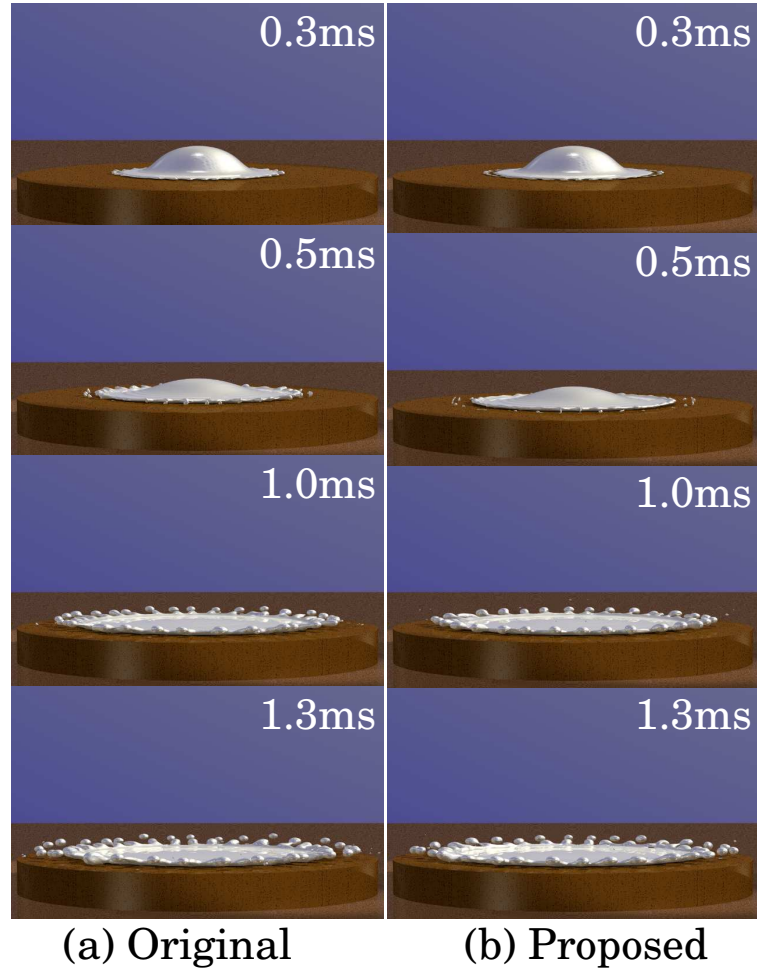

Figure 16: A comparison between the numerical results by the original method (a) and proposed method (b). The corresponding images of the experiment can be found in [21]. A distilled water droplet of 1.86 [mm] impacts onto a super hydrophobic substrate (the equilibrium angle is 163°) which is covered by carbon nanofibers (CNFs). The droplet impact speed is 2.98 [m/s]. A Cartesian grid of $192 \times 192 \times 48$ and $\alpha = 1.5\Delta x$ are used.

droplets and spikes (Fig. 16 (b)) as the original VSIAM3 captured (Fig. 16 (a)). These numerical results have shown at least qualitative agreement with the experiment. The corresponding images of the experiment can be found in [21]. The proposed VSIAM3 has maintained the robustness which the original VSIAM3 has even after significant reduction of numerical viscosity.

3.7   Free surface flows with particles

Finally we conducted numerical simulations of free surface flows with particles as a possible application to Non-Newtonian flows using the proposed VSIAM3. In those simulations, surface tension was not taken into account. DEM (Distinct Element Method) [4, 32, 17, 16] was used for particle dynamics. For the detail of the method to simulate interactions among particles and fluids, see [35]. In these simulations, the densities $\rho_{liquid} = 1000$ kg/m^3, $\rho_{particle} = 500$ kg/m^3, $\rho_{air} = 1.25$ kg/m^3, viscosities $\mu_{liquid} = 1.0 \times 10^{-3}$ Pa·s, $\mu_{air} = 1 \times 10^{-6}$ Pa·s and gravity 9.8 m/s^2 were used. A Cartesian grid of $64 \times 64 \times 64$ was used.

Figures 17 and 18 show numerical results of free surface flows with 8 particles and 27 particles, respectively. Particles fell onto the liquid surface as interacting with air, liquid, other partciles and side wall. The proposed VSIAM3 can robustly simulate interactions among air, particle and liquid.

4   Summary

We proposed an efficient multidimensional implementation of VSIAM3. Although the original VSIAM3 could not capture lid-driven cavity flows of Re>1000 with the Cartesian grid of 128×128, the proposed VSIAM3 could well capture lid-driven cavity flows up to Re=7500. In comparisons with experiments of free surface flows, the proposed VSIAM3 could simulate droplets collision and separation of We=40 with lower numerical resolution (Δ=D/8) than that of the original VSIAM3. The proposed VSIAM3 could capture droplet splashing as the original VSIAM3 did. We also simulated free surface flows with particles as possible Non-Newtonian flow applications. These numerical results have shown that the proposed VSIAM3 could reduce numerical viscosity without losing robustness of the original VSIAM3. The proposed VSIAM3 can be used for various fluid problems including Non-Newtonian flows.
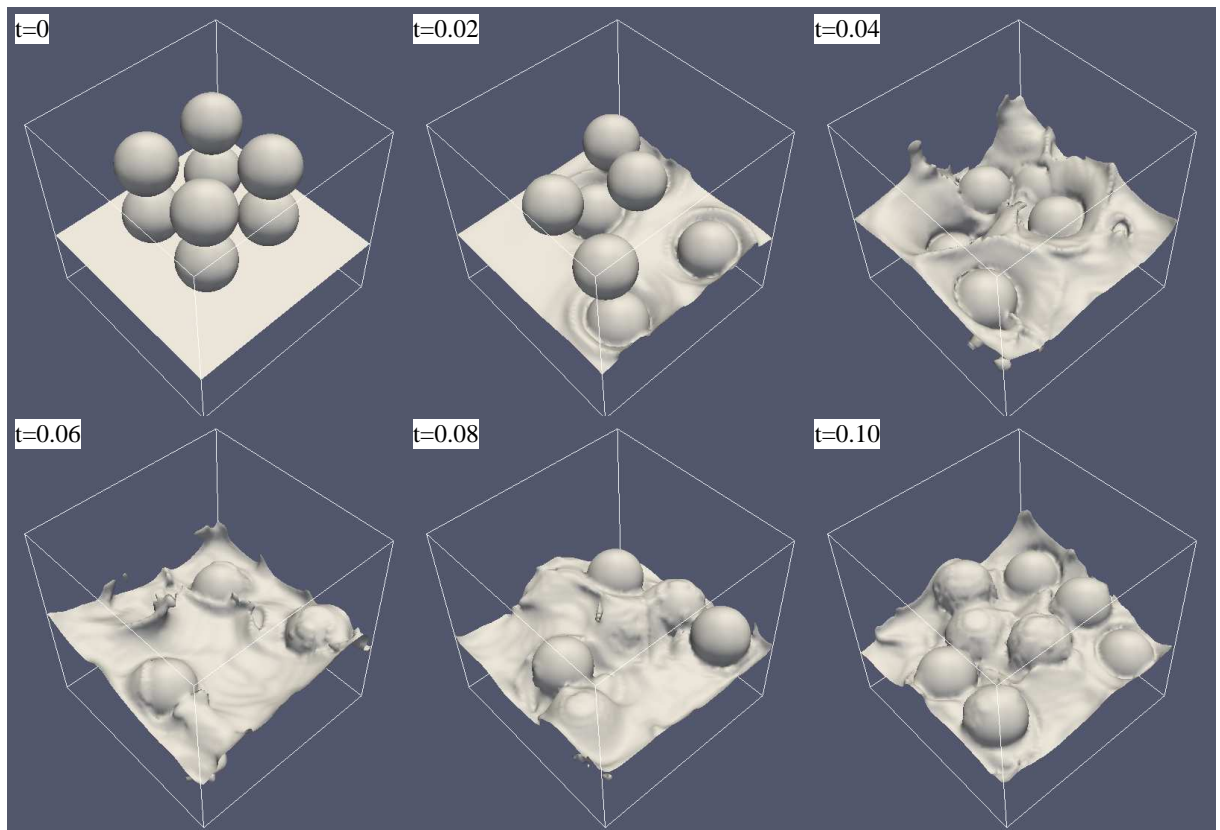
Figure 17: 3D numerical simulation of interaction among air, liquid and 8 particles. A Cartesian grid of $64 \times 64 \times 64$ was used.
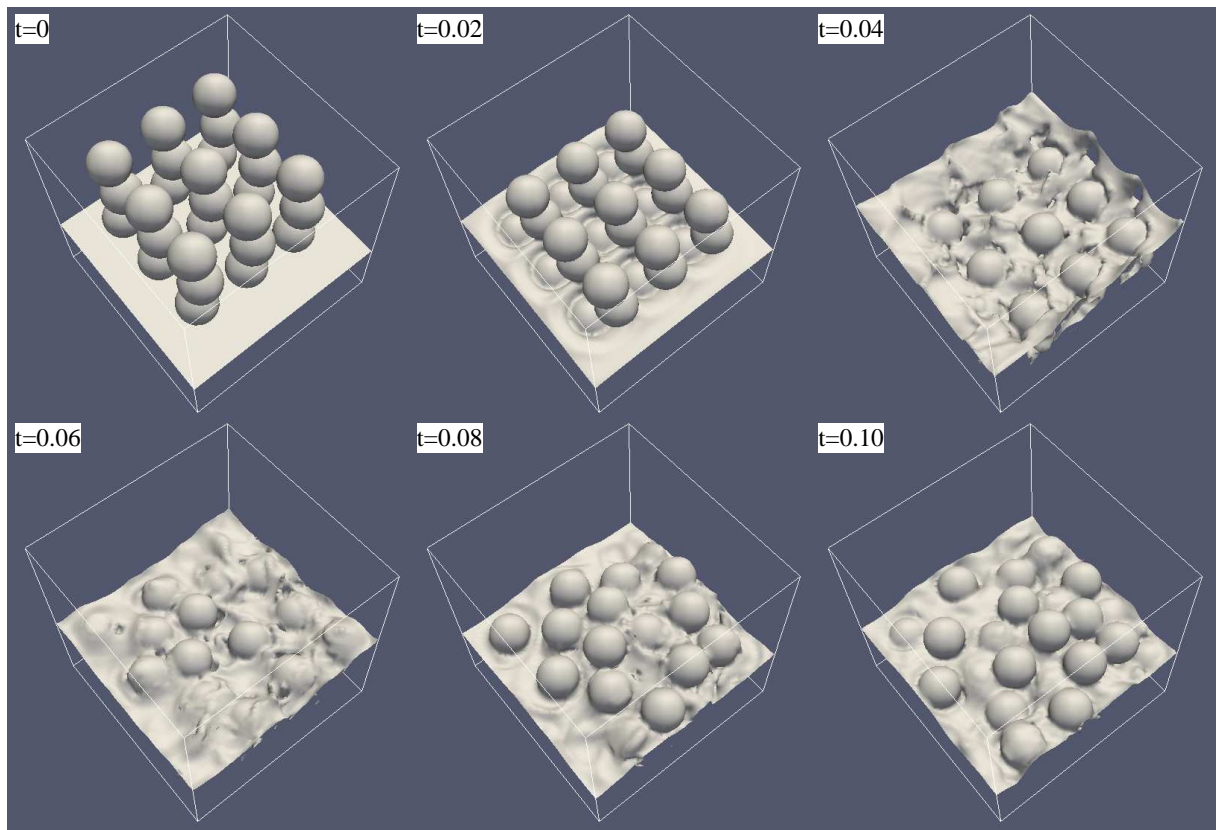
Figure 18: 3D numerical simulation of interaction among air, liquid and 27 particles. A Cartesian grid of $64 \times 64 \times 64$ was used.

5 Acknowledgments

References

[1] M. Al-Mosallam and K. Yokoi. Efficient implementation of volume/surface integrated average-based multi-moment method. *International Journal of Computational Methods*, 14(02):1750010, 2017.

[2] N. Ashgriz and J. Y. Poo. Coalescence and separation in binary collisions of liquid drops. *Journal of Fluid Mechanics*, 221:183–204, 1990.

[3] J. B. Bell, P. Colella, and H. M. Glaz. A second-order projection method for the incompressible navier-stokes equations. *Journal of Computational Physics*, 85(2):257 – 283, 1989.

[4] P. A. Cundall and O. D. L. Strack. A discrete numerical model for granular assemblies. *Gotechnique*, 29(1):47–65, 1979.

[5] U. Ghia, K. Ghia, and C. Shin. High-re solutions for incompressible flow using the navier-stokes equations and a multigrid method. *Journal of Computational Physics*, 48(3):387 – 411, 1982.

[6] A. Harten, B. Engquist, S. Osher, and S. R. Chakravarthy. Uniformly high order accurate essentially non-oscillatory schemes, III. *Journal of Computational Physics*, 71(2):231 – 303, 1987.

[7] C. Hirt and B. Nichols. Volume of fluid (vof) method for the dynamics of free boundaries. *Journal of Computational Physics*, 39(1):201 – 225, 1981.

[8] S. Ii, K. Sugiyama, S. Takeuchi, S. Takagi, Y. Matsumoto, and F. Xiao. An interface capturing method with a continuous function: The thinc method with multi-dimensional reconstruction. *Journal of Computational Physics*, 231(5):2328 – 2358, 2012.

28

[9] G.-S. Jiang and C.-W. Shu. Efficient implementation of weighted ENO schemes. *Journal of Computational Physics*, 126(1):202 – 228, 1996.

[10] J. Li. Calcul d'interface affine par morceaux. *Comptes rendus de l'Académie des sciences. Série II, Mécanique, physique, chimie, astronomie*, 320(8):391–396, 1995.

[11] Q. Li, S. Omar, X. Deng, and K. Yokoi. Constrained interpolation profile conservative semi-lagrangian scheme based on third-order polynomial functions and essentially non-oscillatory (cip-csl3eno) scheme. *Communications in Computational Physics*, 22(3):765–788, 2017.

[12] X.-D. Liu, S. Osher, and T. Chan. Weighted essentially non-oscillatory schemes. *Journal of Computational Physics*, 115(1):200 – 212, 1994.

[13] N. Nikolopoulos, A. Theodorakakos, and G. Bergeles. Off-centre binary collision of droplets: A numerical investigation. *International Journal of Heat and Mass Transfer*, 52(19):4160 – 4174, 2009.

[14] N. Onodera, T. Aoki, and K. Yokoi. A fully conservative high-order upwind multi-moment method using moments in both upwind and downwind cells. *International Journal for Numerical Methods in Fluids*, 82(8):493–511, 2016. fld.4228.

[15] S. Osher and J. A. Sethian. Fronts propagating with curvature-dependent speed: Algorithms based on hamilton-jacobi formulations. *Journal of Computational Physics*, 79(1):12 – 49, 1988.

[16] M. Sakai. How should the discrete element method be applied in industrial systems?: A review. *KONA Powder and Particle Journal*, 33:169–178, 2016.

[17] M. Sakai, M. Abe, Y. Shigeto, S. Mizutani, H. Takahashi, A. Vir, J. R. Percival, J. Xiang, and C. C. Pain. Verification and validation of a coarse grain model of the dem in a bubbling fluidized bed. *Chemical Engineering Journal*, 244:33 – 43, 2014.

[18] M. Sussman and E. G. Puckett. A coupled level set and volume-of-fluid method for computing 3d and axisymmetric incompressible two-phase flows. *Journal of Computational Physics*, 162(2):301 – 337, 2000.

[19] M. Sussman, P. Smereka, and S. Osher. A level set approach for computing solutions to incompressible two-phase flow. *Journal of Computational Physics*, 114(1):146 – 159, 1994.

[20] S. Tanguy and A. Berlemont. Application of a level set method for simulation of droplet collisions. *International Journal of Multiphase Flow*, 31(9):1015 – 1035, 2005.

[21] P. Tsai, S. Pacheco, C. Pirat, L. Lefferts, and D. Lohse. Drop impact upon micro- and nanostructured superhydrophobic surfaces. *Langmuir*, 25(20):12293–12298, 2009. PMID: 19821629.

[22] F. Xiao. Unified formulation for compressible and incompressible flows by using multi-integrated moments I: one-dimensional inviscid compressible flow. *Journal of Computational Physics*, 195(2):629 – 654, 2004.

[23] F. Xiao, R. Akoh, and S. Ii. Unified formulation for compressible and incompressible flows by using multi-integrated moments II: Multi-dimensional version for compressible and incompressible flows. *Journal of Computational Physics*, 213(1):31 – 56, 2006.

[24] F. Xiao, Y. Honma, and T. Kono. A simple algebraic interface capturing scheme using hyperbolic tangent function. *International Journal for Numerical Methods in Fluids*, 48(9):1023–1040, 2005.

[25] F. Xiao, A. Ikebata, and T. Hasegawa. Numerical simulations of free-interface fluids by a multi-integrated moment method. *Computers and Structures*, 83(67):409 – 423, 2005. Frontier of Multi-Phase Flow Analysis and Fluid-StructureFrontier of Multi-Phase Flow Analysis and Fluid-Structure.

[26] F. Xiao, X. D. Peng, and X. S. Shen. A finite-volume grid using multimoments for geostrophic adjustment. *Monthly Weather Review*, 134(9):2515–2526, 2006.

[27] F. Xiao and T. Yabe. Completely conservative and oscillationless semi-lagrangian schemes for advection transportation. *Journal of Computational Physics*, 170(2):498 – 522, 2001.

[28] F. Xiao, T. Yabe, X. Peng, and H. Kobayashi. Conservative and oscillation-less atmospheric transport schemes based on rational functions. *Journal of Geophysical Research: Atmospheres*, 107(D22):ACL 2–1–ACL 2–11, 2002. 4609.

[29] T. Yabe, R. Tanaka, T. Nakamura, and F. Xiao. An exactly conservative semi-lagrangian scheme (CIP-CSL) in one dimension. *Monthly Weather Review*, 129(2):332–344, 2001.

[30] S. Yamashita, C. Chen, K. Takahashi, and F. X. and. Large scale numerical simulations for multi-phase fluid dynamics with moving interfaces. *International Journal of Computational Fluid Dynamics*, 22(6):405–410, 2008.

[31] K. Yokoi. Numerical method for complex moving boundary problems in a cartesian fixed grid. *Phys. Rev. E*, 65:055701, May 2002.

[32] K. Yokoi. Numerical method for interaction between multiparticle and complex structures. *Phys. Rev. E*, 72:046713, Oct 2005.

[33] K. Yokoi. Efficient implementation of THINC scheme: A simple and practical smoothed VOF algorithm. *Journal of Computational Physics*, 226(2):1985 – 2002, 2007.

[34] K. Yokoi. A numerical method for free-surface flows and its application to droplet impact on a thin liquid layer. *Journal of Scientific Computing*, 35(2):372–396, 2008.

[35] K. Yokoi. Numerical method for interaction among multi-particle, fluid and arbitrary shape structure. *Journal of Scientific Computing*, 46(2):166–181, 2011.

[36] K. Yokoi. Numerical studies of droplet splashing on a dry surface: triggering a splash with the dynamic contact angle. *Soft Matter*, 7:5120–5123, 2011.

[37] K. Yokoi. A practical numerical framework for free surface flows based on CLSVOF method, multi-moment methods and density-scaled CSF model: Numerical simulations of droplet splashing. *Journal of Computational Physics*, 232(1):252 – 271, 2013.

[38] K. Yokoi. A density-scaled continuum surface force model within a balanced force formulation. *Journal of Computational Physics*, 278:221 – 228, 2014.

[39] K. Yokoi, R. Onishi, X.-L. Deng, and M. Sussman. Density-scaled balanced continuum surface force model with a level set based curvature interpolation technique. *International Journal of Computational Methods*, 13(04):1641004, 2016.

[40] K. Yokoi, D. Vadillo, J. Hinch, and I. Hutchings. Numerical studies of the influence of the dynamic contact angle on a droplet impacting on a dry surface. *Physics of Fluids*, 21(7):072102, 2009.

366   [41] S. T. Zalesak. Fully multidimensional flux-corrected transport algorithms for fluids. *Journal of Com-*

367   *putational Physics*, 31(3):335 – 362, 1979.